



Metabolic alkalinity release from large port facilities (Hamburg, Germany) and impact on coastal carbon storage

Mona Norbistrath^{1,2}, Johannes Pätsch^{1,3}, Kirstin Dähnke¹, Tina Sanders¹, Gesa Schulz^{1,4}, Justus E. E. van Beusekom¹, Helmuth Thomas^{1,2}

¹Helmholtz-Zentrum Hereon, Institute of Carbon Cycles, Geesthacht, 21502, Germany

²Carl von Ossietzky University Oldenburg, Institute for Chemistry and Biology of the Marine Environment, Oldenburg, 26129, Germany

³University Hamburg, Institute of Oceanography, Hamburg, 20146, Germany

⁴University Hamburg, Institute of Geology, Center for Earth System Research and Sustainability (CEN), Hamburg, 20146, Germany

Correspondence to: Mona Norbistrath (mona.norbistrath@hereon.de)

Abstract

Metabolic activities in estuaries, especially these of large rivers, exert profound impact on downstream coastal biogeochemistry. Here, we unravel the contribution of large industrial port facilities to these impacts and show that metabolic activity in the Hamburg port (Germany) increases total alkalinity (TA) and dissolved inorganic carbon (DIC) runoff to the North Sea. We explained this activity to be fueled by the imports of particulate inorganic and organic carbon (PIC, POC) and particulate organic nitrogen (PON) from the upstream Elbe River, resulting in maximum 90 % TA generation due to CaCO₃ dissolution in the entire estuary. The remaining 10 % can be attributed to a TA generation by anaerobic metabolic processes such as denitrification of remineralized PON, or other pathways. The Elbe Estuary as a whole adds approximately 15 % to the overall DIC and TA runoff. Both the magnitude and partitioning among these processes appear to be sensitive to climate and anthropogenic changes, and affects coastal CO₂ storage capacity.

1 Introduction

Human activities have increased nutrient and organic matter (OM) fluxes to the coastal ocean e.g. (Howarth et al., 1996). Estuaries play an important role in modifying these fluxes for instance by retaining part of the nitrogen fluxes through denitrification (Howarth et al., 2011; Frankignoulle et al., 1998; Seitzinger, 1988; Smith and Hollibaugh, 1993). Since estuaries have an intense biogeochemical cycling, the outer estuary typically acts as a sink of CO₂; the inner estuary is often a source (Borges et al., 2006; Cai and Wang, 1998; Frankignoulle et al., 1998).

Deep estuaries and semi-enclosed seas, such as the Gulf of St. Lawrence or the Baltic Sea, are mostly permanently stratified, which means that they have a strong memory effect due to ventilation time scales of the subsurface waters that are beyond the annual scale. Such waterbodies thus have a high storage capacity for carbon species such as DIC and nutrients e.g. phosphorus,



and may hold oxygen deficits (Mucci et al., 2011) leading to high N retention (De Jonge et al., 1994). Compared to deep estuaries, shallow ones like the Elbe Estuary, are usually well ventilated (Pein et al., 2021; Abril et al., 2002), have a strong benthic-pelagic coupling due to vertical exchange, and respond directly to seasonal forcing.

The Elbe Estuary is located in the northern part of Germany and is about 140 km long. It encompassing an area that begins at the weir in Geesthacht (Elbe stream km 586), crosses the port of Hamburg (Elbe stream km 623) and discharges near Cuxhaven (Elbe stream km 727) into the North Sea, a semi-enclosed shelf sea of the eastern North Atlantic (Fig. 1). The North Sea influences the estuary with its strong tidal cycles, resulting in a semi-diurnal tidal range of 3.6 m in the port of Hamburg (Amann et al., 2012), the third largest port in Europe, and provides a continuous exchange of fresh and marine water.

Eutrophication (e.g. from agricultural fertilizers and wastewater) can cause large phytoplankton blooms both in rivers and in the coastal zone (Hardenbicker et al., 2016). Whose decay increases oxygen consumption (Spieckermann et al., 2021; Schöl et al., 2014), and may lead to declining oxygen levels in bottom water, and possibly hypoxia in estuaries and coastal zones (Große et al., 2016; Howarth et al., 2011; Mucci et al., 2011; Thomas et al., 2009; Frankignoulle et al., 1996; Nixon, 1995). Just upstream of the port of Hamburg, dredging activities have increased the depth from around 5 m to about 20 m to guarantee accessibility of large seagoing vessels. Here, a hotspot of organic matter turnover exists (Pein et al., 2021; Sanders et al., 2018; Schöl et al., 2014). Increasing depths favor seasonal stratification, and sedimentary structures in the port area favor the formation of oxygen-poor or even hypoxic zones (Pein et al., 2021; Kerner, 2007), which are essential for anaerobic metabolic processes that use terminal electron acceptors other than O_2 (e.g. NO_3^- , Fe_3^+ , Mn_4^+ , SO_4^{2-}) to respire organic matter. These metabolic processes release alkalinity in varying stoichiometries (Hu and Cai, 2011; Wolf-Gladrow et al., 2007; Chen and Wang, 1999; Brewer and Goldman, 1976). The resulting reduced products (e.g. N_2 , H_2S , Fe_2^+) can be transported back into the water column. If such reduced products, with the exception of N_2 , can be reoxidized in the water column, any increase in alkalinity from the generation will be consumed. Reduced products can escape reoxidation via permanent burial (e.g. FeS_2 (pyrite)), or via escape to the atmosphere (e.g. N_2). In addition to anaerobic processes, dissolution of calcium carbonate ($CaCO_3$) also generates alkalinity in a TA:DIC ratio of 2:1, which can be reversed by precipitation (Chen and Wang, 1999). For the purpose of this paper, we consider $CaCO_3$ dissolution as a metabolic process favored by lower pH, e.g. bacterial degradation of organic matter, leading to generation of alkalinity. Earlier studies (Francescangeli et al., 2021; Kempe, 1982) confirm the hydrochemical conditions favoring $CaCO_3$ dissolution in the lower Elbe Estuary.

We shed light on the biogeochemical cycling of TA, DIC and in particular nitrate and employ an approach that combines observational and modeling techniques (Schwichtenberg et al., 2020). We want to answer the questions of how much metabolic alkalinity is released from the Elbe Estuary into downstream coastal waters of the North Sea, and how their CO_2 uptake changes under altered metabolic alkalinity inputs as a consequence of climate and anthropogenic changes.



2 Methods

2.1 Study site and observed parameters

2.1.1 Study site

65 This study based on samples that we collected during a cruise (LP20190603) on RV *Ludwig Prandtl* on two consecutive days
 in June 2019 during ebb tide. We sampled from the German Bight around the island of Scharhörn upstream to Oortkaten
 situated in the riverine part of the estuary (Fig. 1). We took surface water (1.2 m depth) samples every 20 minutes out of the
 flow-through FerryBox system (Petersen et al., 2011) that concurrently provides the required physical parameters such as
 salinity, temperature and oxygen. Water depth in the Elbe Estuary was around 15-20 m but sharply decreased to 5 m upstream
 70 Elbe stream km 620. For mass balance calculations, we separated the Elbe Estuary in 6 boxes, indicated by the lines in Fig. 1,
 of which box 1 (upstream the Hamburg port) and box 6 (North Sea) act as boundary conditions.

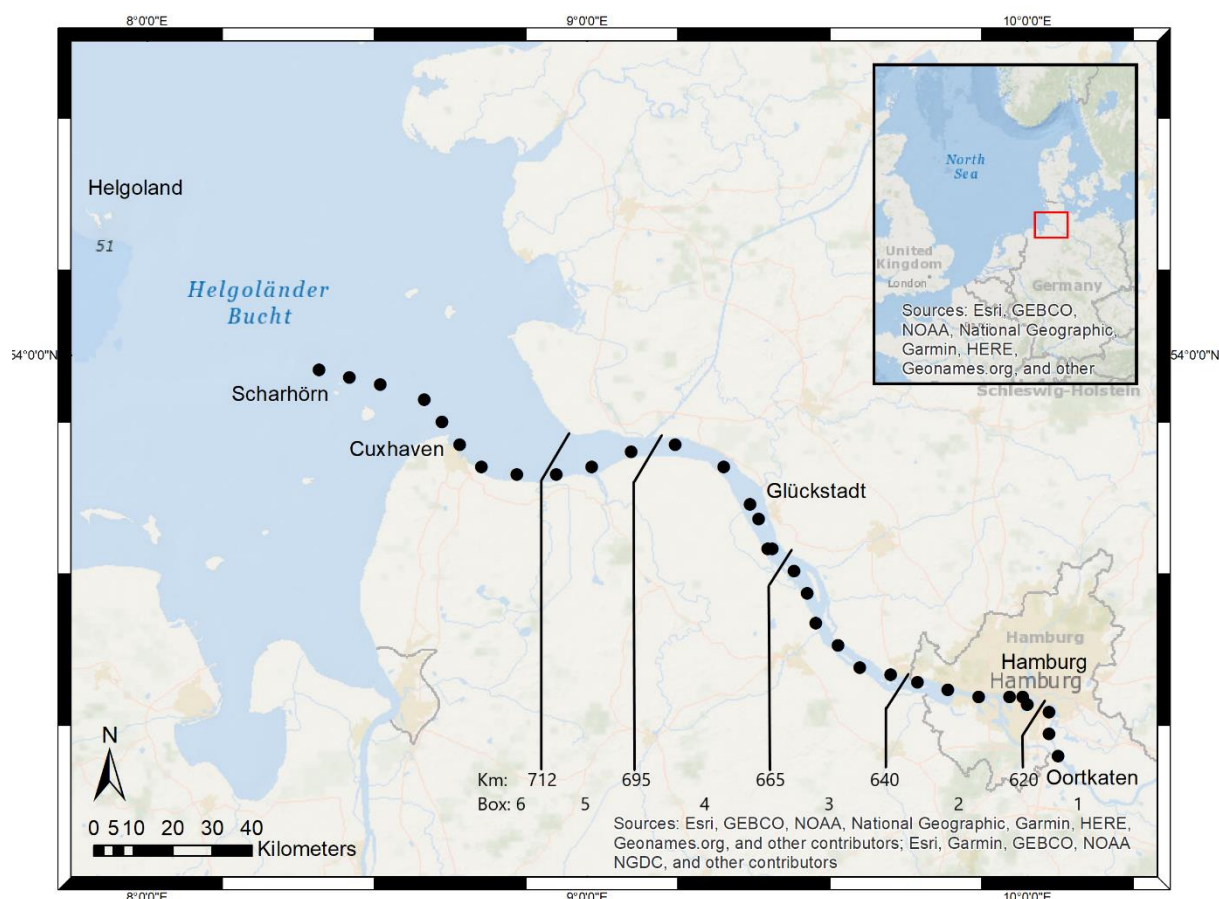




Figure 1. Study site. The Elbe Estuary with sampling stations in June 2019 (dots) and the spatial separation of the estuary for the mass balance calculation (lines), whereby box 2 indicates the port of Hamburg in the upper estuary, box 3 and box 4 in the middle estuary, and box 5 in the lower estuary.

2.1.2 TA and DIC

First, water samples for total alkalinity (TA) and dissolved inorganic carbon (DIC) measurements were filled in 300 mL BOD (biological oxygen demand) bottles and preserved with 300 μL saturated mercuric chloride (HgCl_2) to stop biological activity. We sealed the bottles with ground-glass stoppers, Apiezon® type M grease, free of air bubbles and protected them against opening with plastic caps. Samples were stored in a cool place in the dark until measured.

We performed the measurements of TA and DIC at Helmholtz-Zentrum Hereon using a VINDTA 3C (Versatile Instrument for the Determination of Total dissolved inorganic carbon and Alkalinity, marianda - marine analytics and data). VINDTA 3C measures TA by potentiometric and DIC by coulometric titration, respectively (Shadwick et al., 2011). We used certified reference material (CRM batch # 187) provided by A. G. Dickson (Scripps Institution of Oceanography) to calibrate TA and DIC measurements and ensured a precision of $\pm 2 \mu\text{mol kg}^{-1}$.

2.1.3 Nutrients and stable nitrate isotopes

Samples for nutrients and stable isotopes of nitrate (NO_3^-) were collected concurrently with TA and DIC samples, to measure the concentration and the isotopic composition of nitrate respectively. We collected three 15 mL Falcon tubes for triplicate nutrient measurements, and one 100 mL PE bottle (acid-washed overnight with 10 % HCl) for stable isotope analysis. Samples were filtered through pre-combusted GF/F filters, and then frozen for onshore analyses.

We used a continuous flow automated nutrient analyzer (AA3, SEAL Analytical) and a standard colorimetric technique (Hansen and Koroleff, 2007) to measure concentrations of dissolved nitrate (NO_3^-), nitrite (NO_2^-) and phosphate (PO_4^{3-}), and ammonium (NH_4^+) with a fluorometric method (Kérouel and Aminot, 1997), in triplicate.

We applied the denitrifier method (Casciotti et al., 2002; Sigman et al., 2001) to determine the stable isotope ratios of $\delta^{15}\text{N}$ and $\delta^{18}\text{O}$ of nitrate. We used denitrifying *Pseudomonas aureofaciens* (ATCC#13985), which lacks nitrous oxide reductase activity. The bacteria reduced nitrate and nitrite in the filtered water sample to nitrous oxide (N_2O). The N_2O produced was measured using a GasBench II coupled to an isotope mass spectrometer (Delta Plus XP, Fisher Scientific). Concurrently, we used two international standards (USGS34, $\delta^{15}\text{N-NO}_3^- = -1.8 \text{ ‰}$, $\delta^{18}\text{O-NO}_3^- = -27.9 \text{ ‰}$; IAEA, $\delta^{15}\text{N-NO}_3^- = +4.7 \text{ ‰}$, $\delta^{18}\text{O-NO}_3^- = +25.6 \text{ ‰}$) and one internal standard ($\delta^{15}\text{N-NO}_3^- = +7.6 \text{ ‰}$, $\delta^{18}\text{O-NO}_3^- = +24.4 \text{ ‰}$) for data correction in each run. The standard deviation for standards and samples was $<0.2 \text{ ‰}$ ($n = 4$) for $\delta^{15}\text{N-NO}_3^-$ and $<0.5 \text{ ‰}$ ($n = 4$) $\delta^{18}\text{O-NO}_3^-$. The nitrite concentration of the samples was usually less than 5 %. When it exceeded this threshold, nitrite in the samples was removed with Sulfamic Acid (4 % Sulfamic Acid in 10 % HCl) prior to analysis (Granger and Sigman, 2009).

Variations in the natural abundance of stable isotopes are represented as relative differences in isotope ratios. The isotope ratio R is the ratio of heavy to light isotopes. Since isotope differences are very small, the delta- δ -notation is used to describe the



105 isotopic composition of samples (Eq. 1). Therefore, the isotopic ratio of a sample (R_{sample}) is given relative to the ratio of an internationally accepted reference material ($R_{\text{reference}}$). Atmospheric N_2 and Vienna Standard Mean Ocean Water (VSMOW) are the reference materials for nitrogen and oxygen, respectively. The delta- δ -notation is calculated as follows:

$$\delta (\text{‰}) = \left(\frac{R_{\text{sample}} - R_{\text{reference}}}{R_{\text{reference}}} \right) \times 1000 \quad (1)$$

We identified the nitrate sources river upstream from the minimum isotope values at Elbe stream km 705 using Eq. 2. We
 110 focused on the upper fresh water part of the estuary to identify the isotope values and the source of the additional nitrate (δ_{ad}) added to the estuary between Elbe stream km 609 and 705. We used a simple mixing model (Sanders et al., 2018) with the $\delta^{15}\text{N}$ and $\delta^{18}\text{O}$ values and associated nitrate concentrations (C):

$$\delta_{\text{ad}} = \frac{((\delta_{705} \times C_{705}) - (\delta_{609} \times C_{609}))}{(C_{705} - C_{609})} \quad (2)$$

2.1.4 Ancillary parameters

115 We used pre-combusted (4 h, 450 °C) GF/F filters to sample for particulate organic carbon (POC) and particulate organic nitrogen (PON) concentrations. First, the filters were measured for total carbon (TC) as a bulk sample. Then, the filters were acidified 3 times with 1 N HCl and measured again for POC. The particulate inorganic carbon (PIC) was derived from TC-POC. The filters were measured with a CHN-elemental analyzer (Eurovector EA 3000, HEKAtech GmbH) in the Institute of Geology, University Hamburg. The measurements were calibrated against the standards Sulfanilamide ($C = 41.84 \%$, $N =$
 120 16.27%) und Acetanilide ($C = 71.09 \%$, $N = 10.36 \%$).

The oxygen data were directly measured with the FerryBox, and calibrated with reference to parallel samples analyzed using the Winkler method.

The water depths that we used for the mass balances (see below) were measured during the cruise with the on board Acoustic Doppler Current Profiler (WorkHorse Broadband ADCP 1200kHz, Firmware Version 51.40.) (Cysewski et al., 2018).

125 2.2 Gas flux calculation

As an input function for the mass balances (see below), we estimated CO_2 and O_2 gas exchange (F) between the atmosphere and water. We used the following equation:

$$F_{\text{gas}} = k_{\text{gas}} \times (d_{\text{gas}}) \quad (3)$$

130 where k_{gas} is the transfer velocity of the gases (O_2 and CO_2), and d_{gas} is the difference between the atmospheric and aquatic concentration, calculated as follows:

$$d_{\text{gas}} = [\text{gas}]_{\text{at 100\% saturation}} - [\text{gas}]_{\text{observed}} \quad (4)$$

The CO_2 concentration of the sample (observed) was computed from DIC, TA, salinity and temperature using the CO_2SYS program (Lewis and Wallace, 1998) and the dissociation constants for fresh water (Millero, 1979). The CO_2 concentration of the sample corresponds the mentioned $p\text{CO}_2$. The CO_2 concentration (at 100 % saturation) was obtained from TA and the



135 global atmospheric CO₂ saturation of $416 \pm 0.13 \mu\text{atm}$ (Dlugokencky and Tans, 2021) by using the same previously mentioned program and constants.

The transfer velocity was calculated after Wanninkhof (2014) as follows:

$$k_{\text{gas}} = \frac{0.251 \times (U_{10})^2}{\left(\frac{Sc}{Sc_{\text{ref}}}\right)^{-0.5}} \quad (5)$$

140 where 0.251 is the coefficient of gas transfer, U_{10} is the wind speed in m sec^{-1} measured at 10 m height (provided by DWD (2020)), Sc is the Schmidt number, the kinematic viscosity of water divided by the diffusion coefficient of the gas (Wanninkhof, 2014) and Sc_{ref} is the Sc value relative to the reference conditions of the gas at 20 °C in fresh water, which is 510 for O₂ and 600 for CO₂. The uncertainty of the flux calculation has been estimated to 20 % (Wanninkhof, 2014; Watson et al., 2009).

2.3 Mass balances

2.3.1 Box model approach

145 To balance the net dissolved budgets of TA, DIC, NO₃⁻ and O₂ in the Elbe Estuary, we used a box model approach (Fig. 2) based on our observations. The box model approach allowed us to distinguish conservative contribution from marine and fresh water end-members based on salinity (i. e. baseline), the input and output values as advected transport, and the atmospheric gas exchange (O₂ and CO₂), of the observed parameters TA, DIC, NO₃⁻ and O₂ between and within boxes. The resulting difference is the closing term given as net dissolved budgets, and referred to here as metabolic gains. To attribute the potential
 150 processes affecting metabolic generation, we distinguished between pelagic generation associated with aerobic conditions, i.e., nitrification, which consumes TA, and benthic generation corresponding to anaerobic conditions, where anaerobic metabolic processes generate TA. We defined 6 boxes based on spatial and salinity considerations, with box 1 representing the fresh water (upstream the Hamburg port) and box 6 the coastal ocean (North Sea). Both boxes, 1 and 6 determined the start and end, and were not balanced while acting as boundary conditions. Calculation and end-member properties are shown in Table 1.
 155 Discharge per box was calculated using the observed depths, in combination with an average river discharge value (provided by FGG (2021)) measured from the last tide-free, long term monitoring station Neu Darchau (Elbe stream km 536). Accordingly, we computed the fill time, or in other words the fresh water flushing time of each box, as box volume divided by discharge (Table 1).

We used the following equation to calculate the metabolic gains by assuming a steady state:

$$160 \quad \frac{\delta C}{\delta t} = 0 = F_{\text{Input}} + F_{\text{Output}} + F_{\text{Baseline}} + F_{\text{ASF (O}_2, \text{CO}_2)} + F_{\text{Metabolic}} \quad (6)$$

where F_{Input} is the input value, F_{Output} the output value, F_{Baseline} the salinity corrected baseline value, $F_{\text{ASF (O}_2, \text{CO}_2)}$ the air-sea flux of O₂ and CO₂, respectively, and $F_{\text{Metabolic}}$ the metabolic gain as the closing term.

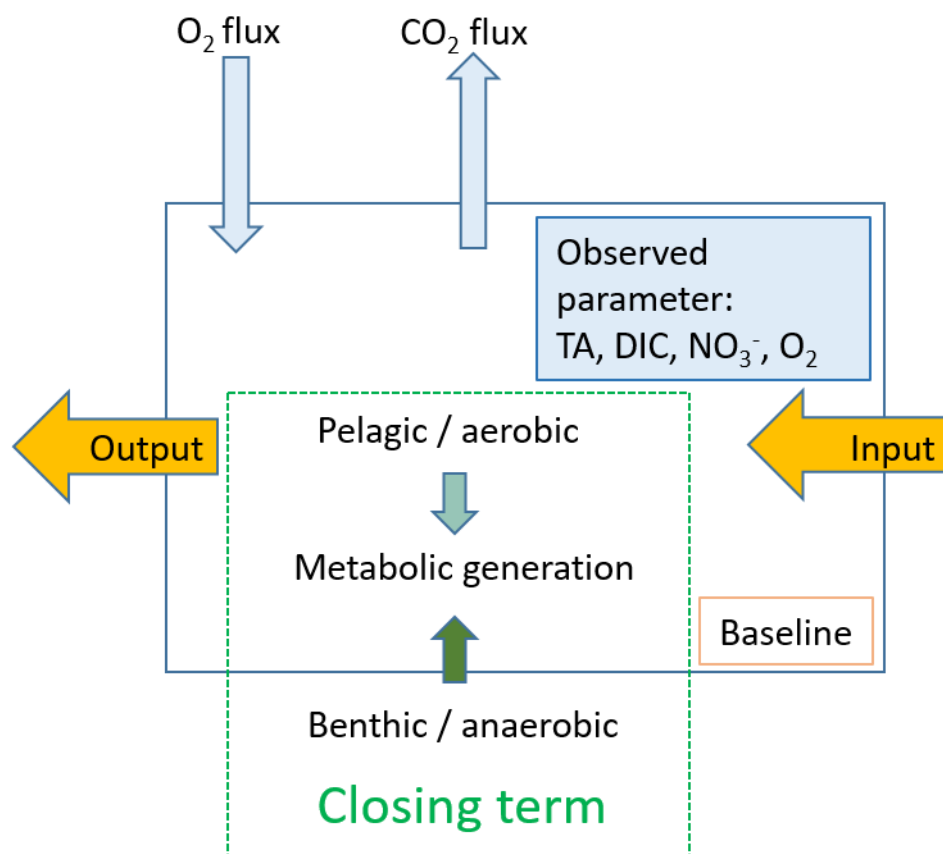


Figure 2. Schematic mass balance approach. We used a box model to balance the net dissolved budgets along the Elbe Estuary. The observed parameters are shown in light blue, the closing term is set as metabolic generation (green), which is fueled by pelagic, i.e. aerobic, and benthic, i.e. anaerobic processes, but without allocating how much of what is generated where. The input and output is shown in yellow, and the latter acts as the input for the downstream box. To complete DIC and O_2 , we included the atmospheric gas exchange. The baseline is calculated assuming conservative mixing of fresh and marine end-members.

Table 1. Elbe Estuary data for the mass balance calculation. The water depths are measured data of the Acoustic Doppler Current Profiler (ADCP) on board of RV *Ludwig Prandtl*, and the river length is based on the Elbe stream km. The river width is based on measurements with Google Maps®, and we used a standardized river width of 2 km for box 3, 4 & 5. The average river discharge on our sampling days was $423 \text{ m}^3 \text{ sec}^{-1}$ (provided by FGG (2021)) measured at the last tide-free long term sampling station in Neu Darchau (Elbe stream km 536). Average box values are given for total alkalinity (TA), dissolved inorganic carbon (DIC), nitrate (NO_3^-) and salinity. For the outer boundary conditions (box 6), we used a maximum salinity of 33.26, and respective TA ($2449 \text{ } \mu\text{mol kg}^{-1}$), DIC ($2132 \text{ } \mu\text{mol kg}^{-1}$), and NO_3^- ($0.1 \text{ } \mu\text{mol L}^{-1}$) values taken on cruise HE541 ($54.062456^\circ \text{ N}$, 8.015919° E), which took place two months later in September 2019 and represents average summer time values for the German Bight. Standard deviation $\pm \text{sd}$ as spatial variability is given when possible.



Species	Unit	Box 1	Box 2	Box 3	Box 4	Box 5	Box 6
Elbe stream km	km	607 - 619	619 - 639	639 - 666	666 - 693	693 - 710	-
Stream width	km	0.3	0.5	2.0	2.0	2.0	-
Stream length	km	12	20	27	27	17	-
Depth	km	0.00493	0.01392	0.016056	0.011999	0.016926	-
Water volume	km ³	0.0177	0.1392	0.8670	0.6479	0.5755	-
Fill time	d	0.4865	3.8094	23.7241	17.7304	15.7468	-
av. TA ± sd	μmol kg ⁻¹	1289 ± 8	1512 ± 40	1630 ± 42	1733 ± 35	1879 ± 21	2449
av. DIC ± sd	μmol kg ⁻¹	1288 ± 30	1589 ± 58	1701 ± 39	1793 ± 29	1896 ± 4	2132
av. NO ₃ ⁻ ± sd	μmol L ⁻¹	74 ± 0	91 ± 6	114 ± 7	139 ± 9	161 ± 6	0.1
av. Salinity ± sd	-	0.41 ± 0.0	0.45 ± 0.0	0.61 ± 0.1	1.07 ± 0.4	5.17 ± 1.4	33.26

The uncertainty of the closing term has been estimated by using the analytical measurement precision of 2 μmol kg⁻¹ for DIC and TA, 0.5 μmol L⁻¹ for NO₃⁻, and 5 % for O₂ (Petersen et al., 2011). The gas exchange was considered with an uncertainty of 20 % (Wanninkhof, 2014; Watson et al., 2009). The river discharge uncertainty was 5 % (Léonard et al., 2000) and was added to the error in the end. The analytical measurement precision of POC and PON was 0.05 % and 0.005 %, respectively (Gaye et al., 2022), calculated from the average box 1 values. The analytical errors were calculated with the following equation per parameter and box:

$$X = (\sum_i x_i^2)^{0.5} \quad (7)$$

where X is the combined error and x_i are the errors of the individual observations.

2.3.2 TA source attribution

In order to assess the total alkalinity gains in the entire Elbe Estuary, we compared the mass balance gains with measured riverine POM properties.

By using the imported riverine PIC and POC, we derived the maximum amount TA fueled by CaCO₃ dissolution as source, and estimated the remaining amount of PIC transported downstream.

In order to estimate the TA gain that can be fueled by CaCO₃ dissolution, we considered the observed metabolic DIC, the average imported PIC:TC (particulate inorganic carbon:total carbon) ratio (0.29 ± 0.05), and the TA:DIC ratio for CaCO₃ dissolution (2) (Chen and Wang, 1999). To get the remaining DIC generated by e.g. organic matter respiration (POC), we multiplied the metabolic DIC gain by 0.71 ($1 - 0.29 = 0.71$). To arrive at the corresponding TA that was not fueled by CaCO₃ dissolution, we subtracted the TA fueled by CaCO₃ dissolution from the entire metabolic TA gain. We performed all calculations per box.

In order to estimate the amount of PIC that is transported through the estuary and not used for TA generation by CaCO₃ dissolution, we used the imported PIC and the previously calculated corresponding TA. The following boxes then do not refer



200 to the imported PIC, but to the product of the previous box that correspond to the unused transported PIC. In case of negative values such as in box 4, we set the transported PIC in the following calculation to 0.

For the coupling of carbon and nitrogen, we used the imported PON to estimate the amount that is transported unused through the Elbe Estuary, and to estimate whether or not riverine PON income is sufficient to generate NO_3^- and TA.

For estimating the TA generation fueled by denitrification that we attribute here to imported riverine PON, we calculated the amount of PON that is available for denitrification by subtracting the nitrified PON (i.e. entire estuarine metabolic NO_3^- gain) of the imported PON (box 1). With the latter calculated PON available for denitrification, the ratio of TA:DIC resulting from denitrification (0.9) (Chen and Wang, 1999), and the entire TA gain that is not fueled by PIC, we calculated the possible TA gain of PON that could be generated in the estuary without the occurrence of nitrification.

210 To estimate the amount of PON that can be transported downstream, we used the imported PON, the sum of the NO_3^- gain of the mass balances, the previously calculated TA gain that was not fueled by PIC, and the TA:DIC ratio (0.9) for denitrification. The following boxes then do not refer to the imported PON, but to the product of the previous box. In case of negative values such as in box 4, we set the transported PON in the following calculation to 0.

2.4 Biogeochemical simulations

For estimating the effects of metabolic produced alkalinity in the estuary on the North Sea and the continental shelf, we applied the 3D-ECOHAM model (Schwichtenberg et al., 2020). Pätsch and Kühn (2008) first described the ECOHAM model domain for this study (see their Fig. 1). Meteorological forcing for both models were derived from the ERA5 reanalysis dataset (Hersbach et al., 2020).

The physical parameters temperature, salinity, horizontal and vertical advection as well as turbulent mixing were calculated using the hydrodynamic model HAMSOM (Backhaus, 1985). This is a baroclinic primitive equation model using the hydrostatic and Boussinesq approximations. Details are described by Backhaus and Hainbucher (1987) and Pohlmann (1996). We run the hydrodynamic model prior to the biogeochemical part. The daily result fields were saved to run the biogeochemical model in offline mode.

The relevant biogeochemical processes and their parameterizations have been detailed in Lorkowski et al. (2012). TA and DIC are computed prognostically. The pelagic biogeochemical part is driven by planktonic production and respiration, calcite formation and dissolution, pelagic and benthic degradation and remineralization, and also by atmospheric deposition of reactive nitrogen. All of these processes affect TA. The air-sea flux of CO_2 was calculated for the North Sea region between 51°N and 59.5°N according to (Wanninkhof, 2014).

We extracted the year 2001 from the simulation run 1979-2014 for the analysis in this paper. Four different scenarios (50, 86, 100, and 150 % TA load) were run, with the 100 % scenario being the reference scenario with full riverine TA and DIC input. In comparison, the 86 % scenario reflects river input without the metabolic alkalinity generation corresponding to our calculated metabolic TA generation of 14 % throughout the Elbe Estuary. We run two other scenarios, one with a reduced TA load (50 %) and one with an increased TA load (150 %) for a broader comparison. Daily data of fresh water fluxes from 254



rivers discharging into the North Sea were used (Große et al., 2017). Corresponding river load data of nutrients, organic matter, DIC, and TA were applied.

235 3 Results and Discussion

3.1 Salinity, TA, DIC, and nutrient distribution along the estuary

Along the transect through the Elbe Estuary, the salinity varied from 0.40 in the fresh water part (Elbe stream km 609-680), to 27.84 in marine waters in the German Bight. The strongest salinity gradient was observed between Elbe stream km 683 and 715 (box 5, tidal front) with an increase of 10 (Fig. 3a). The limited intrusion in salinity in the fresh water part visible in Fig. 240 3a restricted the clear subdivision of the boxes 1 to 3 in Fig. 3b.

TA and DIC increased from the upper estuary (Elbe stream km 609) to the mouth of the estuary (Fig. 3a). The lowest TA and DIC concentrations were 1281 $\mu\text{mol TA kg}^{-1}$ and 1256 $\mu\text{mol DIC kg}^{-1}$ at 0.41 salinity in Oortkaten, the highest were 2272 $\mu\text{mol TA kg}^{-1}$ and 2016 $\mu\text{mol DIC kg}^{-1}$ at 27.84 salinity around Scharhörn. TA was higher than DIC in marine and brackish water, but in the fresh water part of the estuary, DIC was higher than TA. At a salinity of 6.96, TA and DIC were equal with 245 1922 $\mu\text{mol kg}^{-1}$. The strongest increase in TA is observed in the fresh water part close to 0.40 salinity, between Elbe stream km 609 and extending to Elbe stream km 670 (Fig. 3a). In the outer estuary, TA and DIC increased almost proportional to the salinity gradient without obvious biological impact (Fig. 3a,b).

Nitrate (NO_3^-) concentrations increased from 73 $\mu\text{mol NO}_3^- \text{ L}^{-1}$ near Oortkaten to a maximum of 165 $\mu\text{mol NO}_3^- \text{ L}^{-1}$ in the lower estuary at a salinity of 5.08 (Elbe stream km 705, box 5) (Fig. 3a), which is downstream of the maximum turbidity zone 250 (MTZ is located between Elbe stream km 664-670, not shown). Further, nitrate mixed conservatively with low NO_3^- seawater to 15 $\mu\text{mol NO}_3^- \text{ L}^{-1}$ at km 750.

Ammonium (NH_4^+) reached a pronounced maximum of 15 $\mu\text{mol NH}_4^+ \text{ L}^{-1}$ in the Hamburg port area, upstream of the NO_3^- maximum, while varying in a range around 1 $\mu\text{mol NH}_4^+ \text{ L}^{-1}$ in the remainder of the estuary (Fig. 3a). This maximum coincides with the strongest gradients in DIC and TA and can be attributed to high remineralization rates in the port area, as is also 255 evidenced by high apparent oxygen utilization (AOU) (Fig. 3a).

Phosphate (PO_4^{3-}) trends are comparable to nitrate, with a sharp increase in the Hamburg port area and a maximum concentration of 2 $\mu\text{mol PO}_4^{3-} \text{ L}^{-1}$ in the lower estuary (box 5). Similar to TA and DIC, PO_4^{3-} increased where the Elbe River enters the port area.

The $\delta^{15}\text{N-NO}_3^-$ and $\delta^{18}\text{O-NO}_3^-$ isotopic values were higher in the upper estuary and decreased downstream along the estuary 260 to their respective minima at km 705, coinciding with the NO_3^- maximum. The $\delta^{15}\text{N}$ values ranged from 12.4 ‰ to 17.1 ‰, the $\delta^{18}\text{O}$ values from 5.1 ‰ to 9.1 ‰ in the fresh water part.

The $\delta^{15}\text{N}$ values of suspended particulate matter (SPM) ($\delta^{15}\text{N}_p$) showed a pronounced increase from 6 to 10 ‰ in box 2, indicating an enrichment of heavy isotopes in the particulate matter due to the degradation of particulate organic matter (POM). This strong increase coincides with the ammonium peak and the declining $\delta^{15}\text{N-NO}_3^-$.

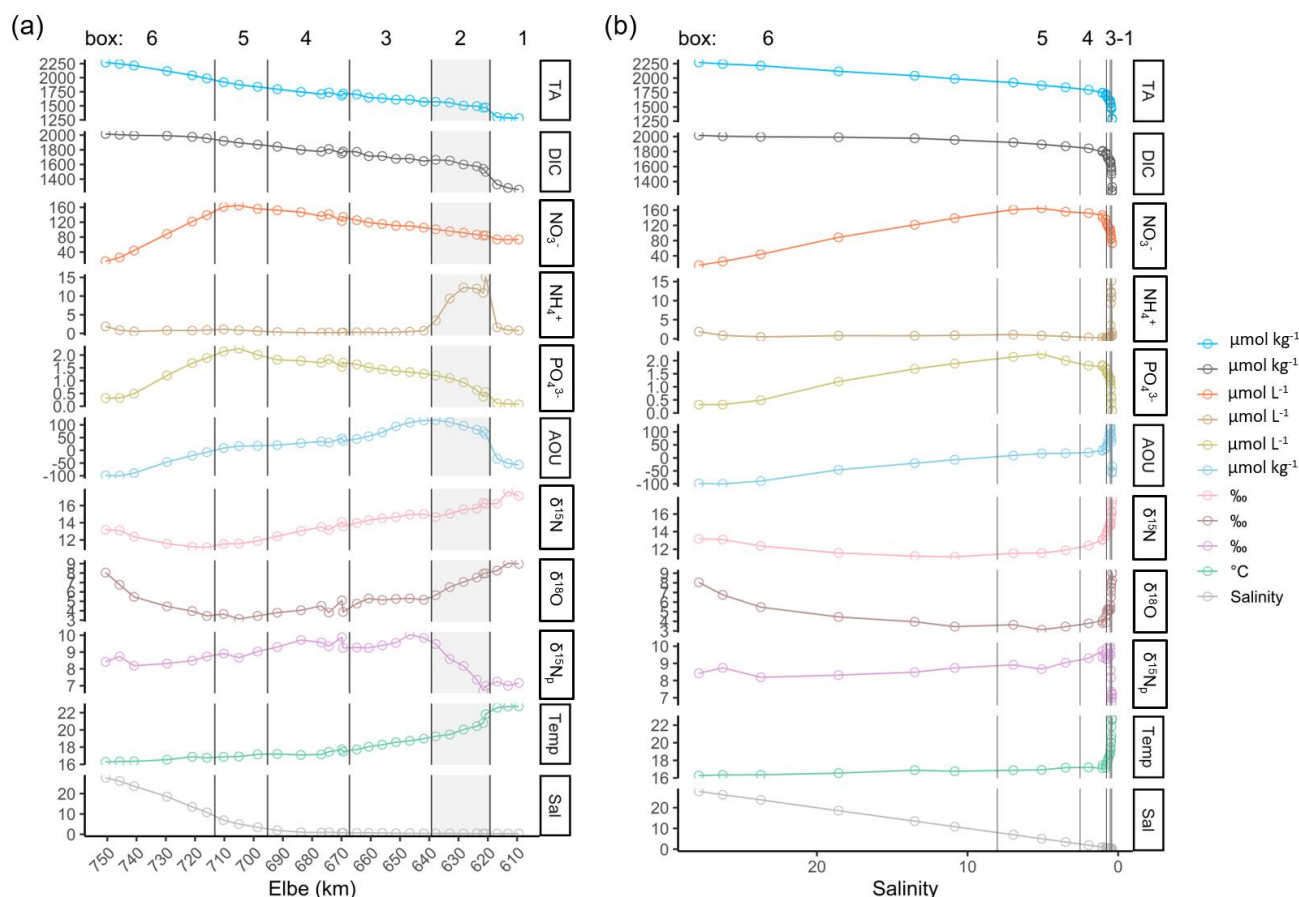


Figure 3. Spatial and salinity dependent observed parameter distribution along the Elbe Estuary. The data are from two days in June 2019. (a) Spatial observed parameter distribution from the inner estuary (Elbe stream km 609, right side) to the German Bight around the island of Scharhörn (computed Elbe stream km 750, left side). Total alkalinity (TA), dissolved inorganic carbon (DIC), nitrate (NO_3^-), ammonium (NH_4^+), phosphate (PO_4^{3-}), apparent oxygen utilization (AOU), delta values of nitrate isotopes ($\delta^{15}\text{N}$) and ($\delta^{18}\text{O}$) of filtered water, and suspended particulate matter ($\delta^{15}\text{N}_p$), temperature (Temp) in °C, and salinity (Sal) are shown. The vertical lines indicate the designated boxes for the mass balance calculation, in which the inner boundary (box 1) is on the right side of the plot, followed by the shaded box 2 with the Hamburg port area (upper estuary), boxes 3 and 4 (middle estuary), 5 (lower estuary), and the outer, marine boundary (box 6) on the left side of the plot. (b) Salinity dependent observed parameter distribution. Note the different y-axis scales within the different panels of both plots.

3.2 Metabolic activity in the port

The North Sea's carbonate system is affected by coastal areas (Schwichtenberg et al., 2020), necessitating a specific investigation of estuarine based TA generation and an estimation of its impact on the oceanic CO_2 uptake capacity. In order to determine the TA, DIC, and O_2 related metabolic activity in the Elbe Estuary, we estimated the air-sea gas exchange of CO_2



and O_2 as these are non-advective processes too (Fig. 4a, Table 2) along the Elbe Estuary. Upstream of the port of Hamburg, the pCO_2 was slightly supersaturated ($465 \mu\text{atm } CO_2$) relative to the atmosphere ($416 \mu\text{atm } CO_2$). Highest values of $2074 \mu\text{atm } CO_2$ in Hamburg port water indicate strong CO_2 degassing. Further downstream, the pCO_2 decreased again (Table 2). In other European estuaries a similar pCO_2 pattern was recorded (Frankignoulle et al., 1998)⁴. pO_2 mirrored the pCO_2 evolution along the estuary and both together allowed us to estimate respective sea to air (in case of CO_2) and air to sea (in case of O_2) fluxes (Fig. 4a).

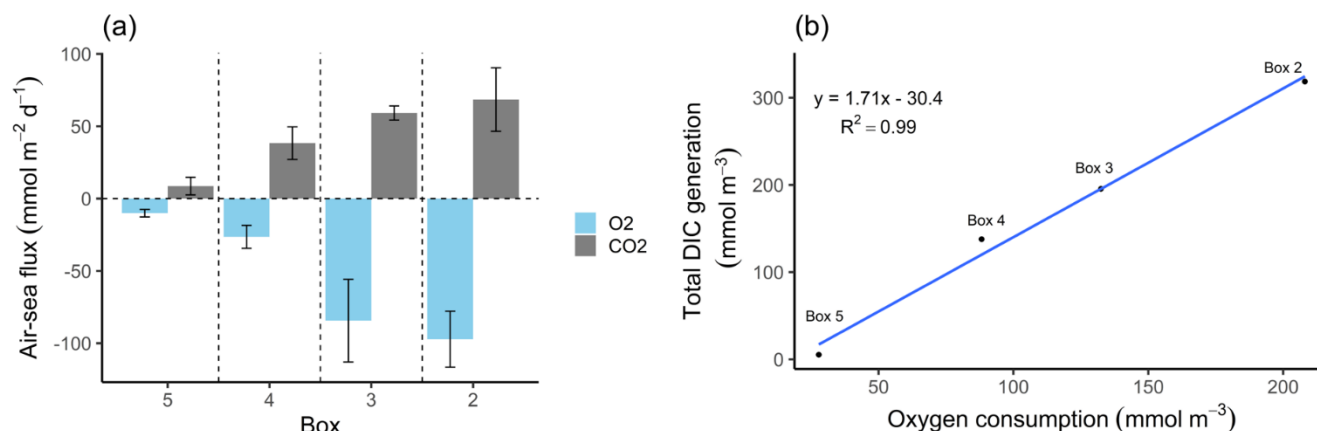


Figure 4. O_2 and CO_2 characteristics. (a) Air-sea fluxes of oxygen (O_2) and carbon dioxide (CO_2) per box, calculated from pO_2 and observed oxygen concentrations, and from pCO_2 values and observed TA, respectively (Table 2). Values are shown with standard deviation represented as spatial variability (error bars). Positive values indicate outgassing, negative values a gas uptake into the water. The Hamburg port area is located in box 2, the lower estuary in box 5. (b) Relationship between metabolic DIC generation and O_2 consumption along the estuary in concentration (mmol m^{-3}). Please note the different parameters in the panels.

The highest metabolic DIC generation and O_2 consumption (Fig. 4a,b, Table 2) occurred in the port of Hamburg, where most of the CO_2 produced remained dissolved, with only a moderate amount being emitted to the atmosphere. The strong metabolic activity is also reflected by the high oxygen influx, driven by low oxygen conditions in the port of Hamburg (Table 2, see for example Amann et al. (2012) & Schöl et al. (2014)). The high slope of 1.71 (Fig. 4b) of DIC and O_2 exceeds the ratio of 0.5 to 1 (e.g. Thomas (2002)), indicating anaerobic or inorganic DIC sources. The remnants of the high metabolic activity in box 2 are transported further downstream to eventually approach equilibrium in the lower estuary (box 5, Fig. 4a,b). Accordingly, here the observed metabolic values obtained for DIC (Fig. 5) and O_2 (AOU, Fig. 3) constitute to a large degree advected signals.

Table 2. Average calculated gas values per box. O_2 concentration is the observed oxygen. O_2 consumption is the amount of oxygen consumed (i.e. AOU + oxygen uptake). Metabolic DIC gen. is the generated DIC. O_2 ASF is the oxygen, and CO_2 ASF is the carbon dioxide air-sea flux along the surface. Positive flux values indicate outgassing, and negative values an absorption into the water. pCO_2 is the partial pressure of carbon dioxide and corresponds to the CO_2 concentration in the water. The standard deviation \pm sd as spatial variability is given



when possible. An uncertainty estimation including the uncertainties of the analytical measurements, the air-sea flux estimation, and the river discharge is given as (\pm absolute errors) by an error propagation (Methods).

Species	Unit	Box 1	Box 2	Box 3	Box 4	Box 5
Elbe stream km	km	607 - 619	619 - 639	639 - 666	666 - 693	693 - 710
O₂ concentration \pm sd	mmol m ⁻³	316 \pm 10	193 \pm 16	210 \pm 30	264 \pm 9	278 \pm 2
O₂ consumption	mmol m ⁻³	-	208 (\pm 15.7)	133 (\pm 30.3)	88 (\pm 21.3)	28 (\pm 20.7)
Metabolic DIC gen.	mmol m ⁻³	-	319 (\pm 5.4)	196 (\pm 18.8)	138 (\pm 12.5)	6 (\pm 4.0)
O₂ ASF \pm sd	mmol m ⁻² d ⁻¹	53 \pm 12	-97 \pm 19	-84 \pm 28	-26 \pm 8	-10 \pm 3
CO₂ ASF \pm sd	mmol m ⁻² d ⁻¹	2 \pm 14	68 \pm 22	59 \pm 5	38 \pm 11	9 \pm 6
pCO₂ \pm sd	µatm	465 \pm 341	2074 \pm 488	1833 \pm 120	1554 \pm 210	713 \pm 208

Using the mass balances, we calculated the net dissolved budgets of TA, DIC, and NO₃⁻, showing only the net gain but no indication of the processes responsible for it. We calculated the highest metabolic gains of both TA and DIC in the Hamburg port area (box 2), identifying this area as the one with the highest metabolic activity (Fig. 5), almost an order of magnitude larger than in the downstream boxes. Accordingly, very high metabolic fluxes, i.e. area and time normalized values, of TA (808 mmol m⁻² d⁻¹) and DIC (1164 mmol m⁻² d⁻¹) were obtained for the Hamburg port area (box 2) (Fig. 5, Table 3), with the downstream values below 150 mmol m⁻² d⁻¹, respectively, further diminishing toward the North Sea with negligible values in box 5. Similarly, the contribution of metabolically generated DIC is higher in the port area, than river downstream where CO₂ equilibration with the atmosphere gains (relative) importance. Compared to the metabolic gains, the air-sea flux (ASF) constitutes only a minor fraction of the metabolic fluxes (Fig. 5). The high release of DIC relative to TA (Fig. 5) are in line with our above result of high pCO₂ in box 2 (Fig. 4a).

In contrast to TA and DIC, the metabolic NO₃⁻ fluxes have a similar magnitude along the estuary, with highest fluxes (63 mmol m⁻² d⁻¹) in the port of Hamburg and lower fluxes (between 16 and 21 mmol m⁻² d⁻¹) in the downstream parts of the estuary. Although the relative difference between box 2 and the downstream boxes is much smaller than for TA and DIC (Fig. 5).

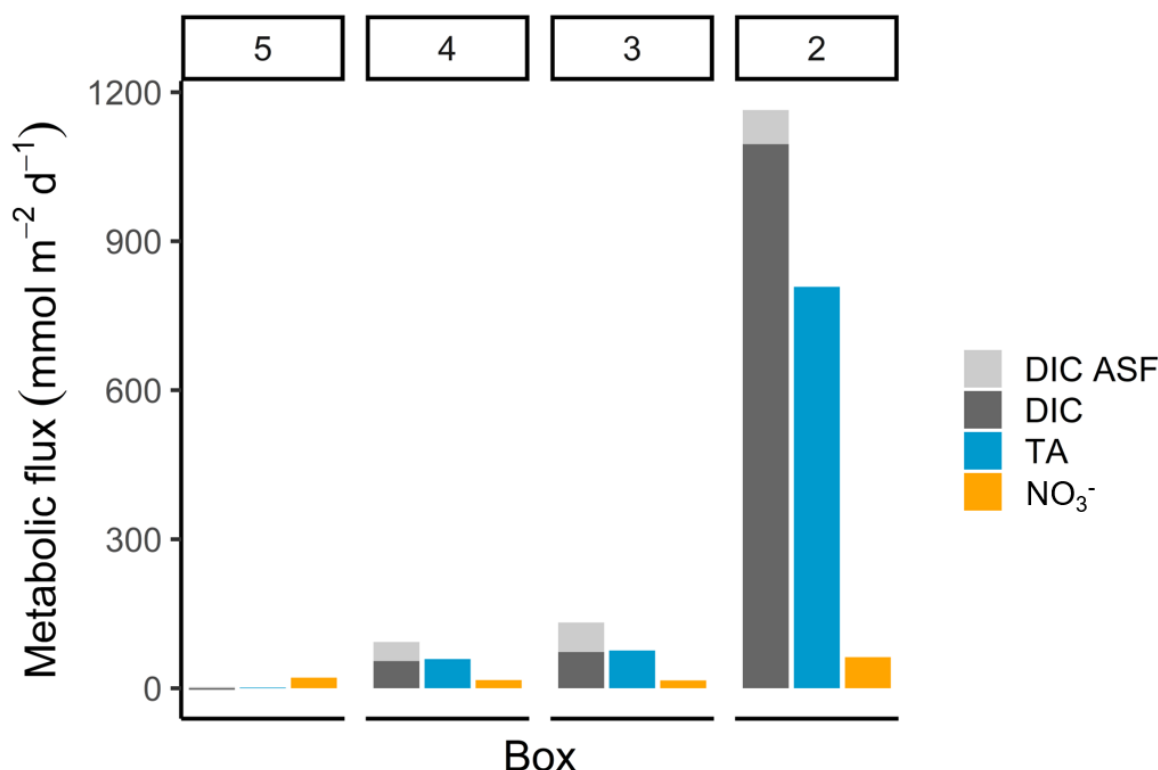


Figure 5. Metabolic fluxes of total alkalinity, dissolved inorganic carbon, and nitrate. The metabolic fluxes of TA (blue), DIC (dark grey) and NO_3^- (orange) in $\text{mmol m}^{-2} \text{d}^{-1}$ are shown, with additionally visualizing the air-sea flux (ASF) contribution to DIC (light grey) to demonstrate the entire generation and their relative magnitude.

325

We estimated the total dissolved metabolic DIC and TA loads from all boxes released into the Elbe Estuary in the North Sea (excluding the air-sea fluxes). Our calculations yield annual metabolic loads of 5.6 Gmol yr^{-1} for TA and 6.5 Gmol yr^{-1} for DIC. In relation to the most recent data from 2017 (Pätsch and Lenhart, 2019), these metabolic loads represent 16 % of the overall DIC ($39.6 \text{ Gmol DIC yr}^{-1}$) and 14 % of the overall TA ($40.3 \text{ Gmol TA yr}^{-1}$) Elbe loads.

330 3.3 Carbon based constraints on TA generation

In order to explain the net total alkalinity gains generated in the Elbe Estuary that were identified with the mass balances, we compared them to imported riverine particulate organic matter (POM) properties from samples taken simultaneously to our Elbe transect (Table 3). We used imported riverine particulate inorganic and organic carbon (PIC, POC) properties to attribute the TA gain fueled by calcium carbonate (CaCO_3) dissolution and to estimate the remaining PIC amount that is transported downstream to identify a possible CaCO_3 deficit along the estuary.

335



We obtained TA generation from CaCO_3 dissolution referring to the metabolic, i.e. POM driven DIC generation multiplied by the observed PIC:TC ratio of 0.29 ± 0.05 (average of entire estuary) of the imported POM. We assumed spontaneous, i.e. maximum dissolution of CaCO_3 , which integrated over the estuary, can contribute up to 90 % of the TA generation and can be considered as an upper bound as we assumed full CaCO_3 dissolution above. The remaining 10 % need to be supplied by other anaerobic, metabolic processes.

In order to estimate the contribution of denitrification as a source for TA generation in the Elbe Estuary and to shed further light on the coupling between TA and nitrogen cycles, we related imported riverine particulate organic nitrogen (PON) to metabolically released NO_3^- .

Without NO_3^- generation by nitrification, we could explain TA generation by denitrification with around 9 % of the overall metabolic TA gain. However, under consideration of both processes occurring in the estuary, we were unable to further attribute denitrification as the entire source for the TA generation in the Elbe Estuary. We identified a nitrogen deficit of riverine imported PON to fuel both NO_3^- generation (i.e. by nitrification) and TA generation (i.e. by denitrification) in boxes 4 and 5 (Table 3) that affect the balance of the entire estuary. This in turn means that lateral NO_3^- sources need to be inferred to balance the nitrogen budget. Similarly, the fairly constant NO_3^- gain along the estuary (Fig. 5), but both decreasing O_2 consumption and DIC generation downstream (Figs. 4b, 5) imply a surplus of nitrate in the downstream part, thus a decoupling between carbon and nitrogen cycling.

To provide further evidence for lateral NO_3^- sources (Kendall et al., 2007; Middelburg and Nieuwenhuize, 2001; Sigman et al., 2001), we employed nitrate stable isotope ($\delta^{15}\text{N}$, $\delta^{18}\text{O}$) signatures. Similar to Dähnke et al. (2008), minimum $\delta^{15}\text{N}$ and $\delta^{18}\text{O}$ values were found in the section with maximum observed NO_3^- concentrations (box 5). The minima were lower than expected from conservative mixing of the North Sea and river end-members and nitrification processes during the 10-30 days downstream transport of the water (see for example Spieckermann et al. (2021)) (Fig. 3a). Nitrification preferentially releases lighter nitrate, depending on the sources for nitrification as evidenced by both decreasing $\delta^{15}\text{N}$ values in NO_3^- and increasing $\delta^{15}\text{N}$ values in SPM (Fig. 3a), but cannot explain the observed local minimum alone. The minimum in isotopic signature is in line with assumed delta values of the added nitrate (Eq. 2) of 7.1 ‰ for $\delta^{15}\text{N}\text{-NO}_3^-$ and -1.6 ‰ for $\delta^{18}\text{O}\text{-NO}_3^-$, respectively (Table 4), which in turn point to an allochthonous, lateral nitrate source. Such can be fueled by soil ammonium oxidation, manure and septic waste (Kendall et al., 2007), which can be identified as nitrogen sources with sufficiently light $\delta^{15}\text{N}$ and $\delta^{18}\text{O}$ characteristics. Although our study implies a lateral NO_3^- source, in contrast to earlier studies (Sanders et al., 2018; Dähnke et al., 2008), we cannot elucidate the corresponding source processes and regions in the context of this study.

Within the entire estuary, the spatial distributions of NO_3^- gain on one hand and the O_2 consumption and metabolic DIC generation on the other hand, show incoherent patterns. We found a decoupling of carbon, nitrogen and oxygen in the middle and lower estuary, with a fairly constant NO_3^- gain along the estuary (Fig. 5), but both decreasing O_2 consumption and DIC generation river downstream (Figs. 4b, 5). Thus, neither O_2 nor DIC reflect the NO_3^- gain, suggesting additional nitrate sources in the downstream fresh water part of the estuary.



Table 3. Mass balance results and POM properties. The mass balance results are shown as metabolic generation (i.e. gains) in concentrations (mmol m^{-3}), in fluxes of total alkalinity (TA), dissolved inorganic carbon (DIC), and nitrate (NO_3^-), respectively (metabolic fluxes are also visualized in Fig. 5), and in kmol d^{-1} . The average carbon:nitrogen (C:N) and particulate inorganic carbon:total carbon (PIC:TC) ratios of suspended particulate matter (SPM) are given per box. The observed imported POC and particulate organic nitrogen (PON) values based on sampled filters in box 1, and the calculated transported values for PON in the other boxes (2-5) (sect. 2.3) are shown. Imported PIC for box 1 was calculated based on imported POC, and transported PIC values were calculated for the other boxes (2-5) (sect. 2.3). DIC fueled by PIC, and TA fueled by PIC give the amount of each that can be fueled of imported and transported PIC. DIC not fueled by PIC, and TA not fueled by PIC give the amount of each that is the remaining and not fueled of imported PIC or i.e. CaCO_3 dissolution. The standard deviation \pm sd as spatial variability is given when possible. An uncertainty estimation for analytical measurements, the air-sea flux estimation and the river discharge is given as (\pm absolute errors) by an error propagation (sect. 2.3). Imported POC, PIC and PON to the estuary was estimated using measured average POC ($596 \pm 52 \mu\text{mol L}^{-1}$), and PON ($91 \pm 8 \mu\text{mol L}^{-1}$) concentrations of SPM ($47 \pm 5 \text{ mg L}^{-1}$), all determined for box 1. PIC is here a synonym for CaCO_3 dissolution as source.

Species	Unit	Box 1	Box 2	Box 3	Box 4	Box 5
Metabolic TA gen.	mmol m^{-3}	-	$221 (\pm 3.6)$	$112 (\pm 3.6)$	$87 (\pm 3.6)$	$1 (\pm 3.6)$
Metabolic DIC gen.	mmol m^{-3}	-	$319 (\pm 5.4)$	$196 (\pm 18.8)$	$138 (\pm 12.5)$	$6 (\pm 4.0)$
Metabolic NO_3^- gen.	mmol m^{-3}	-	$17 (\pm 0.9)$	$23 (\pm 0.9)$	$24 (\pm 0.9)$	$20 (\pm 0.9)$
Metabolic TA flux	$\text{mmol m}^{-2} \text{d}^{-1}$	-	$808 (\pm 13.3)$	$76 (\pm 2.5)$	$59 (\pm 2.5)$	$1 (\pm 3.9)$
Metabolic DIC flux	$\text{mmol m}^{-2} \text{d}^{-1}$	-	$1164 (\pm 19.6)$	$132 (\pm 12.7)$	$93 (\pm 8.5)$	$6 (\pm 4.3)$
Metabolic NO_3^- flux	$\text{mmol m}^{-2} \text{d}^{-1}$	-	$63 (\pm 3.3)$	$16 (\pm 0.6)$	$17 (\pm 0.6)$	$21 (\pm 1.0)$
Av. C:N \pm sd	-	6.6 ± 0.1	7.1 ± 1.1	7.9 ± 0.5	7.9 ± 0.4	7.5 ± 0.4
Av. PIC:TC \pm sd	-	0.286 ± 0.25	0.192 ± 5.33	0.294 ± 0.62	0.314 ± 0.25	0.365 ± 0.33
Metabolic NO_3^-	kmol d^{-1}	-	625.3	857.5	893.5	723.0
Metabolic DIC	kmol d^{-1}	-	11644.3	7146.7	5036.9	196.2
Metabolic TA	kmol d^{-1}	-	8083.7	4090.6	3178.7	44.9
Imported POC	kmol d^{-1}	21788.9 (± 11.4)	-	-	-	-
Imported PON	kmol d^{-1}	3322.9 (± 0.2)	1219.7 (± 0.2)	422.7 (± 0.2)	-756.7 (± 0.2)	-646.5 (± 0.2)
Imported PIC	kmol d^{-1}	6318.8 (± 3.3)	5883.9 (± 3.3)	1738.8 (± 3.3)	-1182.6 (± 3.3)	-113.8 (± 3.3)
DIC fueled by PIC	kmol d^{-1}	-	3376.8 (± 196.7)	2072.5 (± 687.0)	1460.7 (± 457.2)	56.9 (± 147.7)
DIC not fueled by PIC	kmol d^{-1}	-	8267.4 (± 196.7)	5074.2 (± 687.0)	3576.2 (± 457.2)	139.3 (± 147.7)
TA fueled by PIC	kmol d^{-1}	-	6753.7 (± 196.7)	4145.1 (± 687.0)	2921.4 (± 457.2)	113.8 (± 147.7)
TA not fueled by PIC	kmol d^{-1}	-	1330.1 (± 237.4)	-54.5 (± 699.7)	257.3 (± 476.2)	-68.9 (± 198.7)

Table 4. Added nitrate values. The initial values and the changes of the nitrate concentration ($\mu\text{mol L}^{-1}$) and its associated stable isotopes (δ values in ‰) between Elbe stream km 609 and 705 are shown.

NO_3^- [$\mu\text{mol L}^{-1}$]		NO_3^- increase		$\delta^{15}\text{N-NO}_3^-$ [‰]			$\delta^{18}\text{O-NO}_3^-$ [‰]		
609	705	[$\mu\text{mol L}^{-1}$]	[%]	609	705	Added $\delta^{15}\text{N-NO}_3^-$	609	705	Added $\delta^{18}\text{O-NO}_3^-$



73.9 164.8 90.8 122.9 17.1 11.5 7.1 8.9 3.1 -1.6

385

3.4 Estuarine carbon release and estimated impact on coastal carbon storage

The impacts of anthropogenic and management activities on estuarine and coastal carbon cycling and CO₂ uptake have frequently been discussed from an aerobic perspective, as for example by Borges and Gypens (2010) for the southern North Sea. Here we attempt to complement this perspective by considering anaerobic processes. We employed a biogeochemical simulation approach (Schwichtenberg et al., 2020) to estimate the impacts of estuarine metabolic TA gains on the carbon cycle and CO₂ uptake capacity in the North Sea. We used this simulation approach to highlight the effect of changing DIC:TA ratios, e.g. due to anthropogenic induced changes, on the carbon storage in coastal oceans. Conceptually, the simulations reflect the relative balance between aerobic and anaerobic respiration of a given amount of organic carbon, such that any reduced alkalinity scenario implies a preference for aerobic processes, and the increased alkalinity scenarios in turn imply a preference of anaerobic processes releasing a given amount of DIC. We applied four scenarios in which we changed the TA loads as input variable, and compared the resulting CO₂ uptake by the North Sea at three different distances from coast. For the first scenario, the reference run (i.e. normal condition), we used the full riverine TA and DIC load that correspond to a TA load of 100 %. For the second scenario, we reduced the TA load to 86 % reflecting the above contribution (14 %) of metabolic alkalinity to the overall alkalinity release by the Elbe Estuary. For further comparisons, we ran scenarios with a reduced TA load to 50 % and an increased TA load to 150 %. We extrapolate these scenarios to 254 rivers that discharge into the North Sea. In particular, the major rivers and estuaries are either associated with a major port (e.g. Antwerp, Rotterdam, London or Bremerhaven), or are generally characterized as a highly turbid and heavily used waterway (e.g. Ems) that, like the Elbe Estuary, provide ideal conditions for anaerobic metabolic pathways.

Under reference conditions (100 % TA), the open North Sea (> 200 km distance from the coastline) absorbs more atmospheric CO₂, with carbon transported in the deeper zones via the continental shelf pump (Thomas et al., 2004), than the coastal zones (100 km distance) (Fig. 6, absolute ASF indicated by bars). This spatial distribution is also visible in the scenarios with reduced TA loads. Assuming a remaining TA load of 50 % and 86 %, we modeled less CO₂ uptake due to reduced metabolic alkalinity generations.

Compared to the reduced TA scenarios, the increased TA scenario (150 %) also has higher CO₂ uptake within each distance, but in spatial distribution, higher CO₂ uptake in coastal areas than in the open North Sea. This indicates that in the 150 % scenario the open North Sea no longer represents the area of strongest CO₂ uptake.

The differences in CO₂ uptake in the North Sea (Fig. 6, difference ASF indicated by lines) between the scenarios with reduced TA (50 & 86 %) and the reference scenario (100 %) decreased with increasing distance from the coast. This change is also reflected in the difference in CO₂ uptake between the scenario with increased TA load (150 %) and the reference scenario, where the difference in CO₂ uptake is higher in the coastal area than in the open ocean. This phenomenon can be partly explained by mixing, as the signal is more diluted the further offshore. Furthermore, CO₂ equilibration continues as waters are



transported offshore (e.g. Burt et al. (2014)), i.e. away from the TA source. The larger differences in CO₂ uptake in coastal areas suggest that the effects of TA input from metabolic processes in rivers are similar in magnitude to the simulated (Fig. 6) and observed (Thomas et al., 2004) air-sea flux itself. Similar evidence has been presented by Burt et al. (2016), who report that benthic sediment release in the southern North Sea shapes, if not dominates, the seasonal variability of the TA system (see also Thomas et al. (2009)).

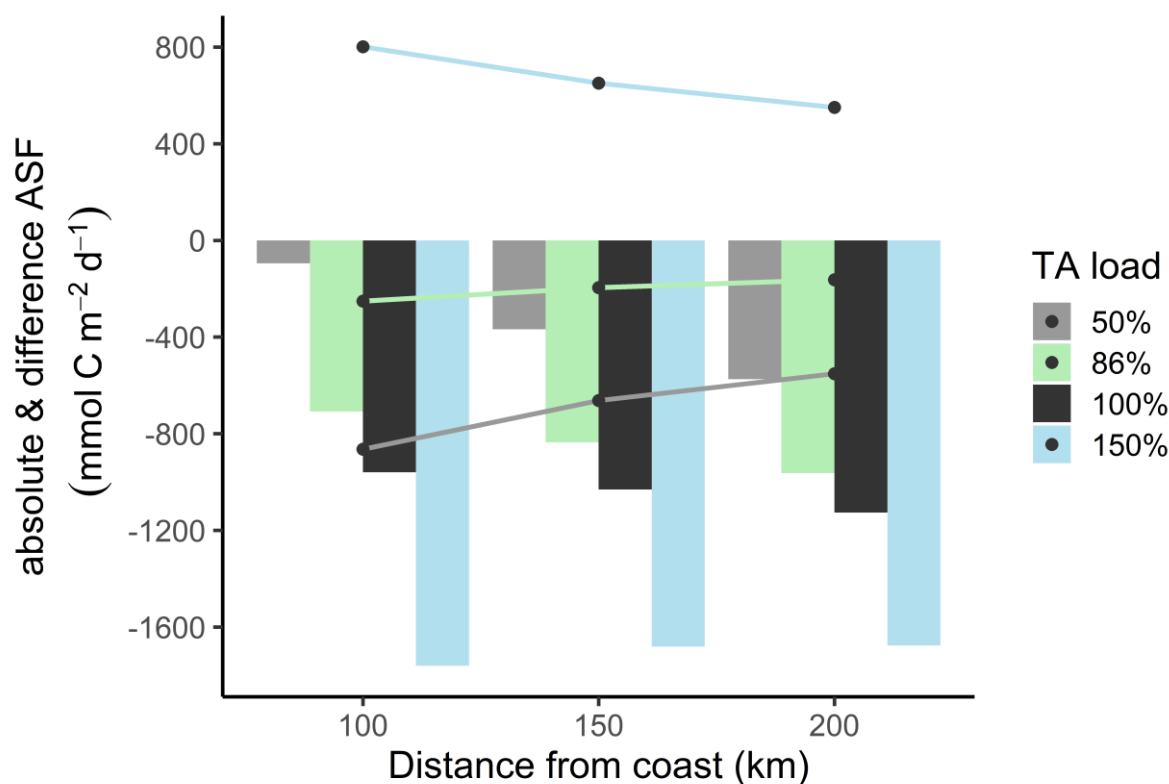


Figure 6. Biogeochemical CO₂ air-sea flux (ASF) simulations at distance from coast. The bars show the annual absolute CO₂ uptake in the water under reduced (50 %, grey) and (86 %, green), normal (100 %, black) and increased (150 %, blue) TA load. The lines visualize the CO₂ uptake difference between the scenarios 50, 86, 150 %, and the reference scenario (100 %).

Next to CO₂ air-sea fluxes, the metabolic TA release from the Hamburg port area could also affect calcifying organisms such as foraminifera that occur in the lower Elbe Estuary. In a recent study, Francescangeli et al. (2021) observed the change of calcite saturation state (Ω_{Ca}) from under- to supersaturation around Elbe km 685 (approx.). Without the respective TA generation, the supersaturated range and thus the habitat of the foraminifera, would clearly be further downstream, if not restricted to the North Sea. For example, at their most saline station (Francescangeli et al. (2021), see their Fig. 2f), corresponding to Elbe stream km 730 in our study, the observed Ω_{Ca} is ~ 3.3 , whereas it would be strongly undersaturated ($\Omega_{Ca} \sim 0.2$) without benthic TA release.



4 Conclusions

435 We observed clear regional differences in the biogeochemistry of the Elbe Estuary. While conservative mixing prevails in the salinity gradient of the lower estuary, metabolic processes dominate the upper, fresh water part with the port of Hamburg. We observed a strong increase of several hundred $\mu\text{mol kg}^{-1}$ of TA and DIC in the Hamburg port (Fig. 3) with vanishing values downstream, and calculated an annual metabolic TA load of about 14 % of the total TA runoff from the Elbe River to the coastal ocean.

440 Mass balances suggest that up to 90 % of the generated TA of the entire estuary could be fueled by imported PIC, i.e. through CaCO_3 dissolution. Anaerobic metabolic processes such as denitrification, iron, manganese, or sulfate reduction could fuel the remaining 10 % of TA generation. Accordingly, estuarine ecosystems appear to be highly susceptible in particular to nutrient management actions that affect the balance of the various metabolic processes to generate TA by controlling NO_3^- availability, as organic carbon and oxygen supply appear in excess or steady, respectively. One could speculate that the reduced organic

445 carbon supply would reduce the importance of anaerobic processes in favor of a relative increase in aerobic respiration. On the other hand, a reduction in NO_3^- for a given organic carbon content would trigger other anaerobic processes (e.g iron or sulfate reduction) that have a higher TA gain per unit of carbon respired than does denitrification (Chen and Wang, 1999). The interplay of the various metabolic processes governs both the release of reduced products and the carbonate system properties in the estuary. For example, the former controls the balance of released gases such as N_2 , N_2O and H_2S , which in

450 turn can have negative effects on the entire estuarine biodiversity, leading to losses in reproduction and habitats of e.g. local fish species (Breitburg et al., 2009; Wu, 2009; Breitburg, 2002; Janas and Szaniawska, 1996). The carbonate system properties regulate the habitable range for example for benthic foraminifera (Francescangeli et al., 2021). We show that the metabolic TA release increases capacity and CO_2 absorption in the German Bight. We postulate that this result may be transferable to other global rivers or estuarine systems, particularly those with large port facilities, and that it could have tangible implications for

455 the ocean's CO_2 uptake capacity on a global scale.

Data availability

The datasets generated during and/or analyzed during the current study are either presented in the study, and are in preparation to be released in accordance with the rules of the funding agency.

Author contributions

460 MN, KD, and HT designed the study. MN did the sampling, sample measurements and analyses, data interpretation and evaluation, and prepared the manuscript. JP did the biogeochemical simulation by using the 3D-ECOHAM model. GS performed stable isotope measurements, data analysis and interpretation, and added to the method description. KD, TS, JP, JEEVB, and HT provided scientific and editorial recommendations. MN wrote the manuscript with input from all co-authors.



Competing interests

465 The authors declare that they have no conflict of interest.

Acknowledgement

This research has been funded by the German Academic Exchange Service (DAAD, project: MOPGA-GRI, grant no. 57429828), which received funds from the German Federal Ministry of Education and Research (BMBF).

We thank our crew of the RV *Ludwig Prandtl* for their helping hands during the sampling campaign. Thanks to Leon Schmidt
 470 for measuring the nutrients, our intern Jeannette Hansen for supporting us with the box model calculation, Linda Baldewein
 for supporting us with the Elbe River kilometer calculation, the working group of biogeochemistry at the Institute of Geology,
 University Hamburg for measuring the filters, and Yoana Voynova for providing the FerryBox data. The oxygen calibration
 samples were collected by Götz Flöser, analyzed by Tanja Pieplow, and processed by Yoana Voynova. The FerryBox
 preparation (optode specific) was done by Martina Gehrung.

References

- Abril, G., Nogueira, M., Etcheber, H., Cabeçadas, G., Lemaire, E., and Brogueira, M.: Behaviour of organic carbon in nine contrasting European estuaries, *Estuarine, coastal and shelf science*, 54, 241-262, 2002.
- Amann, T., Weiss, A., and Hartmann, J.: Carbon dynamics in the freshwater part of the Elbe estuary, Germany: Implications of improving water quality, *Estuarine, Coastal and Shelf Science*, 107, 112-121, 2012.
- 480 Backhaus, J. O.: A three-dimensional model for the simulation of shelf sea dynamics, *Deutsche Hydrografische Zeitschrift*, 38, 165-187, 1985.
- Backhaus, J. O., and Hainbucher, D.: A finite difference general circulation model for shelf seas and its application to low frequency variability on the North European Shelf, in: *Elsevier oceanography series*, Elsevier, 221-244, 1987.
- Borges, A., Schiettecatte, L.-S., Abril, G., Delille, B., and Gazeau, F.: Carbon dioxide in European coastal waters, *Estuarine, Coastal and Shelf Science*, 70, 375-387, 2006.
- 485 Borgesa, A. V., and Gypensb, N.: Carbonate chemistry in the coastal zone responds more strongly to eutrophication than ocean acidification, *Limnology and Oceanography*, 55, 346-353, 2010.
- Breitbart, D.: Effects of hypoxia, and the balance between hypoxia and enrichment, on coastal fishes and fisheries, *Estuaries*, 25, 767-781, 2002.
- 490 Breitbart, D. L., Craig, J. K., Fulford, R. S., Rose, K. A., Boynton, W. R., Brady, D. C., Ciotti, B. J., Diaz, R., Friedland, K., and Hagy, J.: Nutrient enrichment and fisheries exploitation: interactive effects on estuarine living resources and their management, *Hydrobiologia*, 629, 31-47, 2009.
- Brewer, P. G., and Goldman, J. C.: Alkalinity changes generated by phytoplankton growth 1, *Limnology and Oceanography*, 21, 108-117, 1976.
- 495 Burt, W., Thomas, H., Pätsch, J., Omar, A., Schrum, C., Daewel, U., Brenner, H., and de Baar, H.: Radium isotopes as a tracer of sediment-water column exchange in the North Sea, *Global Biogeochemical Cycles*, 28, 786-804, 2014.
- Burt, W., Thomas, H., Hagens, M., Pätsch, J., Clargo, N., Salt, L., Winde, V., and Böttcher, M.: Carbon sources in the North Sea evaluated by means of radium and stable carbon isotope tracers, *Limnology and Oceanography*, 61, 666-683, 2016.
- Cai, W. J., and Wang, Y.: The chemistry, fluxes, and sources of carbon dioxide in the estuarine waters of the Satilla and Altamaha Rivers, Georgia, *Limnology and Oceanography*, 43, 657-668, 1998.
- 500 Casciotti, K. L., Sigman, D. M., Hastings, M. G., Böhlke, J., and Hilkert, A.: Measurement of the oxygen isotopic composition of nitrate in seawater and freshwater using the denitrifier method, *Analytical chemistry*, 74, 4905-4912, 2002.
- Chen, C. T. A., and Wang, S. L.: Carbon, alkalinity and nutrient budgets on the East China Sea continental shelf, *Journal of Geophysical Research: Oceans*, 104, 20675-20686, 1999.



- 505 Cysewski, M., Seemann, J., and Horstmann, J.: Artifacts or Nature? Data Processing and Interpretation of 3D Current Fields Recorded with Vessel Mounted Acoustic Doppler Current Profiler in Different Regions and Conditions, 2018 OCEANS-MTS/IEEE Kobe Techno-Oceans (OTO), 2018, 1-5,
 Dähnke, K., Bahlmann, E., and Emeis, K.: A nitrate sink in estuaries? An assessment by means of stable nitrate isotopes in the Elbe estuary, *Limnology and Oceanography*, 53, 1504-1511, 2008.
- 510 De Jonge, V. N., Boynton, W., D'Elia, C. F., Elmgren, R., and Welsh, R.: Responses to developments in eutrophication in four different North Atlantic estuarine systems, OLSEN & OLSEN, FREDENSBORG, DENMARK., 179-196, 1994.
 Dlugokencky, E., and Tans, P.: Trends in atmospheric carbon dioxide. National Oceanic and Atmospheric Administration, Earth System Research Laboratory (NOAA/ESRL), 2021.
 DWD, Deutscher Wetter Dienst (DWD), Climate Data Center (CDC), https://www.dwd.de/DE/klimaumwelt/cdc/cdc_node.html, 2020.
- 515 FGG, Flussgebietsgemeinschaft (FGG) Elbe, https://www.elbe-datenportal.de/FisFggElbe/content/auswertung/UntersuchungsbereichHydro_start_x.action, 2021.
 Francescangeli, F., Milker, Y., Bunzel, D., Thomas, H., Norbisch, M., Schönfeld, J., and Schmiedl, G.: Recent benthic foraminiferal distribution in the Elbe Estuary (North Sea, Germany): A response to environmental stressors, *Estuarine, Coastal and Shelf Science*, 251, 107198, 2021.
- 520 Frankignoulle, M., Bourge, I., and Wollast, R.: Atmospheric CO₂ fluxes in a highly polluted estuary (the Scheldt), *Limnology and Oceanography*, 41, 365-369, 1996.
 Frankignoulle, M., Abril, G., Borges, A., Bourge, I., Canon, C., Delille, B., Libert, E., and Théate, J.-M.: Carbon dioxide emission from European estuaries, *Science*, 282, 434-436, 1998.
- 525 Gaye, B., Lahajnar, N., Harms, N., Paul, S. A. L., Rixen, T., and Emeis, K.-C.: What can we learn from amino acids about oceanic organic matter cycling and degradation?, *Biogeosciences*, 19, 807-830, 2022.
 Granger, J., and Sigman, D. M.: Removal of nitrite with sulfamic acid for nitrate N and O isotope analysis with the denitrifier method, *Rapid Communications in Mass Spectrometry: An International Journal Devoted to the Rapid Dissemination of Up-to-the-Minute Research in Mass Spectrometry*, 23, 3753-3762, 2009.
- 530 Große, F., Greenwood, N., Kreuz, M., Lenhart, H.-J., Machoczek, D., Pätsch, J., Salt, L., and Thomas, H.: Looking beyond stratification: a model-based analysis of the biological drivers of oxygen deficiency in the North Sea, *Biogeosciences*, 13, 2511-2535, 2016.
 Große, F., Kreuz, M., Lenhart, H.-J., Pätsch, J., and Pohlmann, T.: A novel modeling approach to quantify the influence of nitrogen inputs on the oxygen dynamics of the North Sea, *Frontiers in Marine Science*, 4, 383, 2017.
- Hansen, H., and Koroleff, F.: Determination of nutrients. *Methods of Seawater Analysis: Third, Completely Revised and Extended Edition*. Weinheim, Germany: Wiley-VCH Verlag GmbH, 2007.
- 535 Hardenbicker, P., Weitere, M., Ritz, S., Schöll, F., and Fischer, H.: Longitudinal plankton dynamics in the rivers Rhine and Elbe, *River Research and Applications*, 32, 1264-1278, 2016.
 Hersbach, H., Bell, B., Berrisford, P., Hirahara, S., Horányi, A., Muñoz-Sabater, J., Nicolas, J., Peubey, C., Radu, R., and Schepers, D.: The ERA5 global reanalysis, *Quarterly Journal of the Royal Meteorological Society*, 146, 1999-2049, 2020.
- 540 Howarth, R., Chan, F., Conley, D. J., Garnier, J., Doney, S. C., Marino, R., and Billen, G.: Coupled biogeochemical cycles: eutrophication and hypoxia in temperate estuaries and coastal marine ecosystems, *Frontiers in Ecology and the Environment*, 9, 18-26, 2011.
 Howarth, R. W., Billen, G., Swaney, D., Townsend, A., Jaworski, N., Lajtha, K., Downing, J. A., Elmgren, R., Caraco, N., and Jordan, T.: Regional nitrogen budgets and riverine N & P fluxes for the drainages to the North Atlantic Ocean: Natural and human influences, in: *Nitrogen cycling in the North Atlantic Ocean and its watersheds*, Springer, 75-139, 1996.
- 545 Hu, X., and Cai, W. J.: An assessment of ocean margin anaerobic processes on oceanic alkalinity budget, *Global Biogeochemical Cycles*, 25, 2011.
 Janas, U., and Szaniawska, A.: The influence of hydrogen sulphide on macrofaunal biodiversity in the Gulf of Gdansk, *Oceanologia*, 38, 127-142, 1996.
- Kempe, S.: Valdivia cruise, October 1981: carbonate equilibria in the estuaries of Elbe, Weser, Ems and in the Southern German Bight, *Transport of carbon and minerals in major world rivers*. Univ. Hamburg, 52, 719-742, 1982.
- 550 Kendall, C., Elliott, E. M., and Wankel, S. D.: Tracing anthropogenic inputs of nitrogen to ecosystems, *Stable isotopes in ecology and environmental science*, 2, 375-449, 2007.
 Kerner, M.: Effects of deepening the Elbe Estuary on sediment regime and water quality, *Estuarine, coastal and shelf science*, 75, 492-500, 2007.
- Kérouel, R., and Aminot, A.: Fluorometric determination of ammonia in sea and estuarine waters by direct segmented flow analysis, *Marine Chemistry*, 57, 265-275, 1997.
- 555 Léonard, J., Muetton, M., Najib, H., and Gourbesville, P.: Rating curve modelling with Manning's equation to manage instability and improve extrapolation, *Hydrological sciences journal*, 45, 739-750, 2000.
- Lewis, E., and Wallace, D.: Program developed for CO₂ system calculations, *Environmental System Science Data Infrastructure for a Virtual Ecosystem*, 1998.



- 560 Lorkowski, I., Pätsch, J., Moll, A., and Kühn, W.: Interannual variability of carbon fluxes in the North Sea from 1970 to 2006—Competing effects of abiotic and biotic drivers on the gas-exchange of CO₂, *Estuarine, Coastal and Shelf Science*, 100, 38-57, 2012.
- Middelburg, J., and Nieuwenhuize, J.: Nitrogen isotope tracing of dissolved inorganic nitrogen behaviour in tidal estuaries, *Estuarine, Coastal and Shelf Science*, 53, 385-391, 2001.
- Millero, F. J.: The thermodynamics of the carbonate system in seawater, *Geochimica et Cosmochimica Acta*, 43, 1651-1661, 1979.
- 565 Mucci, A., Starr, M., Gilbert, D., and Sundby, B.: Acidification of lower St. Lawrence Estuary bottom waters, *Atmosphere-Ocean*, 49, 206-218, 2011.
- Nixon, S. W.: Coastal marine eutrophication: a definition, social causes, and future concerns, *Ophelia*, 41, 199-219, 1995.
- Pätsch, J., and Kühn, W.: Nitrogen and carbon cycling in the North Sea and exchange with the North Atlantic—a model study. Part I. Nitrogen budget and fluxes, *Continental Shelf Research*, 28, 767-787, 2008.
- 570 Pätsch, J., and Lenhart, H.: Daily Loads of Nutrients, Total Alkalinity, Dissolved Inorganic Carbon and Dissolved Organic Carbon of the European Continental Rivers for the Years 1977 – 2017, DATA RIVER, Universität Hamburg, 2019.
- Pein, J., Eisele, A., Sanders, T., Daewel, U., Stanev, E. V., Van Beusekom, J. E., Staneva, J., and Schrum, C.: Seasonal Stratification and Biogeochemical Turnover in the Freshwater Reach of a Partially Mixed Dredged Estuary, *Frontiers in Marine Science*, 8, 623714, 2021.
- Petersen, W., Schroeder, F., and Bockelmann, F.-D.: FerryBox-Application of continuous water quality observations along transects in the
- 575 North Sea, *Ocean Dynamics*, 61, 1541-1554, 2011.
- Pohlmann, T.: Predicting the thermocline in a circulation model of the North Sea—Part I: model description, calibration and verification, *Continental Shelf Research*, 16, 131-146, 1996.
- Sanders, T., Schöl, A., and Dähnke, K.: Hot spots of nitrification in the Elbe estuary and their impact on nitrate regeneration, *Estuaries and coasts*, 41, 128-138, 2018.
- 580 Schöl, A., Hein, B., Wyrwa, J., and Kirchesch, V.: Modelling water quality in the Elbe and its estuary—Large Scale and Long Term Applications with Focus on the Oxygen Budget of the Estuary, *Die Küste*, 81 Modelling, 203-232, 2014.
- Schwichtenberg, F., Pätsch, J., Böttcher, M. E., Thomas, H., Winde, V., and Emeis, K.-C.: The impact of intertidal areas on the carbonate system of the southern North Sea, *Biogeosciences*, 17, 4223-4245, 2020.
- Seitzinger, S. P.: Denitrification in freshwater and coastal marine ecosystems: ecological and geochemical significance, *Limnology and oceanography*, 33, 702-724, 1988.
- 585 Shadwick, E., Thomas, H., Gratton, Y., Leong, D., Moore, S., Papakyriakou, T., and Prowe, A.: Export of Pacific carbon through the Arctic Archipelago to the North Atlantic, *Continental Shelf Research*, 31, 806-816, 2011.
- Sigman, D. M., Casciotti, K. L., Andreani, M., Barford, C., Galanter, M., and Böhlke, J.: A bacterial method for the nitrogen isotopic analysis of nitrate in seawater and freshwater, *Analytical chemistry*, 73, 4145-4153, 2001.
- 590 Smith, S., and Hollibaugh, J.: Coastal metabolism and the oceanic organic carbon balance, *Reviews of Geophysics*, 31, 75-89, 1993.
- Spieckermann, M., Gröngroft, A., Karrasch, M., Neumann, A., and Eschenbach, A.: Oxygen Consumption of Resuspended Sediments of the Upper Elbe Estuary: Process Identification and Prognosis, *Aquatic Geochemistry*, 1-25, 2021.
- Thomas, H.: Remineralization ratios of carbon, nutrients, and oxygen in the North Atlantic Ocean: A field databased assessment, *Global Biogeochemical Cycles*, 16, 24-21-24-12, 2002.
- 595 Thomas, H., Bozec, Y., Elkalay, K., and De Baar, H. J.: Enhanced open ocean storage of CO₂ from shelf sea pumping, *Science*, 304, 1005-1008, 2004.
- Thomas, H., Schiettecatte, L.-S., Suykens, K., Koné, Y., Shadwick, E., Prowe, A. F., Bozec, Y., de Baar, H. J., and Borges, A.: Enhanced ocean carbon storage from anaerobic alkalinity generation in coastal sediments, *Biogeosciences*, 6, 267-274, 2009.
- Wanninkhof, R.: Relationship between wind speed and gas exchange over the ocean revisited, *Limnology and Oceanography: Methods*, 12, 351-362, 2014.
- 600 Watson, A. J., Schuster, U., Bakker, D. C., Bates, N. R., Corbière, A., González-Dávila, M., Friedrich, T., Hauck, J., Heinze, C., and Johannessen, T.: Tracking the variable North Atlantic sink for atmospheric CO₂, *Science*, 326, 1391-1393, 2009.
- Wolf-Gladrow, D. A., Zeebe, R. E., Klaas, C., Körtzinger, A., and Dickson, A. G.: Total alkalinity: The explicit conservative expression and its application to biogeochemical processes, *Marine Chemistry*, 106, 287-300, 2007.
- 605 Wu, R. S.: Effects of hypoxia on fish reproduction and development, in: *Fish physiology*, Elsevier, 79-141, 2009.